Differentiating Parkinson's Disease Motor Subtypes Using Automated Volume-Based Morphometry Incorporating White Matter and Deep Gray Nuclear Lesion Load

Eric Fang, MD, FRCR,[1] Chu Ning Ann, BA (Hons),[2] Bénédicte Maréchal, PhD,[3,4,5]

Jie Xin Lim, MA,[6] Shawn Yan Zhi Tan, BSc (Hons),[1] Huihua Li, PhD,[1]

Julian Gan, BSc (Hons), MBA,[7] Eng King Tan, MBBS, MRCP, FRCP, FAMS,[2,8] and

Ling Ling Chan, MBBS, FRCR, FAMS[1,8]*

Background: Periventricular leukoaraiosis may be an important pathological change in postural instability gait disorder (PIGD), a motor subtype of Parkinson's disease (PD). Clinical diagnosis of PIGD may be challenging for the general neurologist.
Purpose: To evaluate 1) the utility of a fully automated volume-based morphometry (Vol-BM) in characterizing imaging diagnostic markers in PD and PIGD, including, 2) novel deep gray nuclear lesion load (GMab), and 3) discriminatory performance of a Vol-BM model construct in classifying the PIGD subtype.
Study Type: Prospective.
Subjects: In all, 23 PIGD, 21 PD, and 20 age-matched healthy controls (HC) underwent MRI brain scans and clinical assessments.
Field Strength/Sequence: 3.0T, sagittal 3D-magnetization-prepared rapid gradient echo (MPRAGE), and fluid-attenuated inversion recovery imaging (FLAIR) sequences.
Assessment: Clinical assessment was conducted by a movement disorder neurologist. The MR brain images were then segmented using an automated multimodal Vol-BM algorithm (MorphoBox) and reviewed by two authors independently.
Statistical Testing: Brain segmentation and clinical parameter differences and dependence were assessed using analysis of variance (ANOVA) and regression analysis, respectively. Logistic regression was performed to differentiate PIGD from PD, and discriminative reliability was evaluated using receiver operating characteristic (ROC) analysis.
Results: Significantly higher white matter lesion load (WMab) ($P < 0.01$), caudate GMab ($P < 0.05$), and lateral and third ventricular ($P < 0.05$) volumetry were found in PIGD, compared with PD and HC. WMab, caudate and putamen GMab, and caudate, lateral, and third ventricular volumetry showed significant coefficients ($P < 0.005$) in linear regressions with balance and gait assessments in both patient groups. A model incorporating WMab, caudate GMab, and caudate GM discriminated PIGD from PD and HC with a sensitivity = 0.83 and specificity = 0.76 (AUC = 0.84).
Data Conclusion: Fast, unbiased quantification of microstructural brain changes in PD and PIGD is feasible using automated Vol-BM. Composite lesion load in the white matter and caudate, and caudate volumetry discriminated PIGD from PD and HC, and showed potential in classification of these disorders using supervised machine learning.
Level of Evidence: 1
Technical Efficacy: Stage 1

PARKINSON'S DISEASE (PD) is a neurodegenerative disorder characterized by a range of motor and nonmotor

features such as resting tremor, bradykinesia, rigidity, postural instability, and neurobehavioral dysfunction.[1] Clinically

heterogeneous phenotypes and variable progression in PD suggest complex underlying microstructural alterations involving multiple brain regions and different networks beyond the nigrostriatal pathway.[2–4] Focal gray matter lesions within the basal ganglia and iron deposition also contribute to the pathophysiology of PD.[5–7] Postural instability gait disorder (PIGD), a motor subtype of PD with predominant balance and gait disturbances, progresses rapidly, with prominent cognitive decline, and has been postulated to be secondary to complication by periventricular leukoaraiosis.[8] In addition, PIGD patients are less responsive to levo-dopamine treatment[9] compared with the tremor dominant PD subtype. Hence, distinguishing the PIGD motor subtype of PD for early intervention and therapeutic management is important.

Morphometric brain studies reporting structural alterations between PD subtypes are typically voxel-based, semiautomated,[4,10,11] and yield inconsistent findings of cortical and subcortical volume alterations.[10–13] None have examined deep gray nuclear lesion load to date.[4,14] This study aimed at evaluating the utility of 1) a fully automated volume-based morphometry, and 2) novel deep gray nuclear lesion load estimation (GMab) in characterizing imaging diagnostic markers in PD and PIGD in relation to clinical correlates. This was then applied to 3) construct a model that could discriminate the PIGD subtype to aid in classification.

Materials and Methods

Study Subjects

This prospective study was conducted in accordance with approved guidelines and regulations of the Institutional Review Board. Informed consent was obtained from all subjects. Sixty-six subjects (25 PIGD, 21 PD, and 20 age- and gender-matched controls) were included in this automated whole-brain morphometric analysis.[15,16] Diagnosis was made by a movement disorders neurologist (E.T.) with more than two decades of clinical experience in the field, following the United Kingdom PD Brain Bank criteria.[17] PIGD is diagnosed based on the widely used clinical classification of the ratio of the mean Unified Parkinson's Disease Rating Scale Motor Scale (UPDRS) tremor to PIGD scores (≤1.0).[1,18] Disease severity was evaluated in the "on state" using UPDRS Part III[19] and modified Hoehn and Yahr Scale.[20] Motor symptoms were assessed using the Tinetti Balance Scale (TBS).[21] No lateralization of motor symptoms was reported. The Abbreviated Mental Test[22] was used to screen for cognitive dysfunction. Vascular risk factors, namely hypertension, diabetes, and hyperlipidemia, were recorded.

Exclusion criteria included secondary Parkinsonism, parkinsonism-plus syndromes,[17] atypical parkinsonism features (suggesting stroke, normal pressure hydrocephalus, or structural lower limb abnormalities), cognitive and organ dysfunction or life-threatening diseases. Secondary parkinsonism refers to symptomatic parkinsonism secondary to other causes such as drug-induced parkinsonism, space-occupying or infective etiologies, whereas parkinson-plus syndromes refer to rapidly progressive neurodegenerative conditions presenting with parkinsonism and additional neurological abnormalities such as autonomic dysfunction,

cerebellar, and eye signs. The patients included in our cohort had a follow-up period of at least 3 years at our Movement Disorders clinics to reduce misdiagnosis and exclude parkinson-plus syndromes. Controls were recruited from healthy volunteers and relatives of patients with no evidence of neurological disorders or cognitive dysfunction.

MRI Acquisition

Magnetic resonance imaging (MRI) brain imaging was performed on a 3T MR scanner (Magnetom Trio, Siemens Healthcare, Erlangen, Germany) with a 12-channel phased array head coil. Sagittal 3D-magnetization-prepared rapid gradient echo (MPRAGE) parameters were: repetition time / echo time / inversion time / flip angle (TR/TE/TI/FA) 2200/3.0/900msec/9 degrees; 240 mm field of view (FOV); 256 × 256 matrix; 0.9 mm slice thickness; 192 slices. A fluid-attenuated inversion recovery imaging (FLAIR) sequence (TR/TE 5000/384 msec; 230 mm FOV; 256 × 256 matrix; 0.9 slice thickness; 192 slices) was used to aid in quality review of abnormal white and gray matter segmentation. Subjects' heads were stabilized with foam padding on both sides. Patients were scanned during their "on" state to reduce motion.

Image Analysis

Automated segmentation of deep gray nuclei, ie, caudate, thalamus, putamen, and pallidum, was performed using the MorphoBox prototype combining atlas-based segmentation and atlas-free tissue classification algorithms.[23,24] Figure 1a–c shows a representation of the processing performed to estimate abnormal white matter (WMab) and deep gray nuclear lesion load (GMab) volumes. Brain tissue classification was performed on a skull-stripped brain by means of a template-free algorithm fitting a 5-class Gaussian mixture model roughly representing ventricular cerebrospinal fluid (CSF), sulcal CSF, cortical gray matter, deep gray matter, and white matter. Model fitting was carried out using a variational expectation-maximization algorithm,[24] which generated an output of five a posteriori probability maps and subsequently converted into three maps corresponding to CSF, gray matter, and white matter by combining the ventricular with sulcal CSF maps and the cortical with deep gray matter maps. WMab was detected by thresholding the difference between posterior and prior white matter probability maps[23] according to a constant value of 0.6. GMab was obtained by summing up CSF a posteriori probabilities over each nucleus mask obtained by atlas propagation.

COMPUTATION OF WMAB AND GMAB. WMab is a relative volumetric measure, where $\text{WMab} = \frac{\text{Abnormal white matter volume}}{\text{Total whole brain gray matter and white matter probabilities}}$. For each deep gray nucleus, absolute volume for each is first computed by summing up gray and white matter probabilities over relevant anatomical masks, eg, Absolute caudate volume = Absolute volume of (gray matter + white matter) probabilities in caudate. Relative deep gray nuclear volume is then normalized over total brain volume, eg, $\text{caudate volumetry} = \frac{\text{Absolute caudate volume}}{\text{Total whole brain gray matter and white matter probabilities}}$. Tissue composition of each deep gray nucleus is also computed, eg, $\text{caudate gray matter} = \frac{\text{Absolute volume of gray matter probabilities in caudate}}{\text{Absolute caudate volume}}$ and $\text{caudate white matter} = \frac{\text{Absolute volume of white matter probabilities in caudate}}{\text{Absolute caudate volume}}$. GMab is obtained by summing up CSF a posteriori probabilities over each nucleus, eg, $\text{caudate GMab} = \frac{\text{Sum of CSF a posteriori probabilities in caudate}}{\text{Absolute caudate volume}}$.
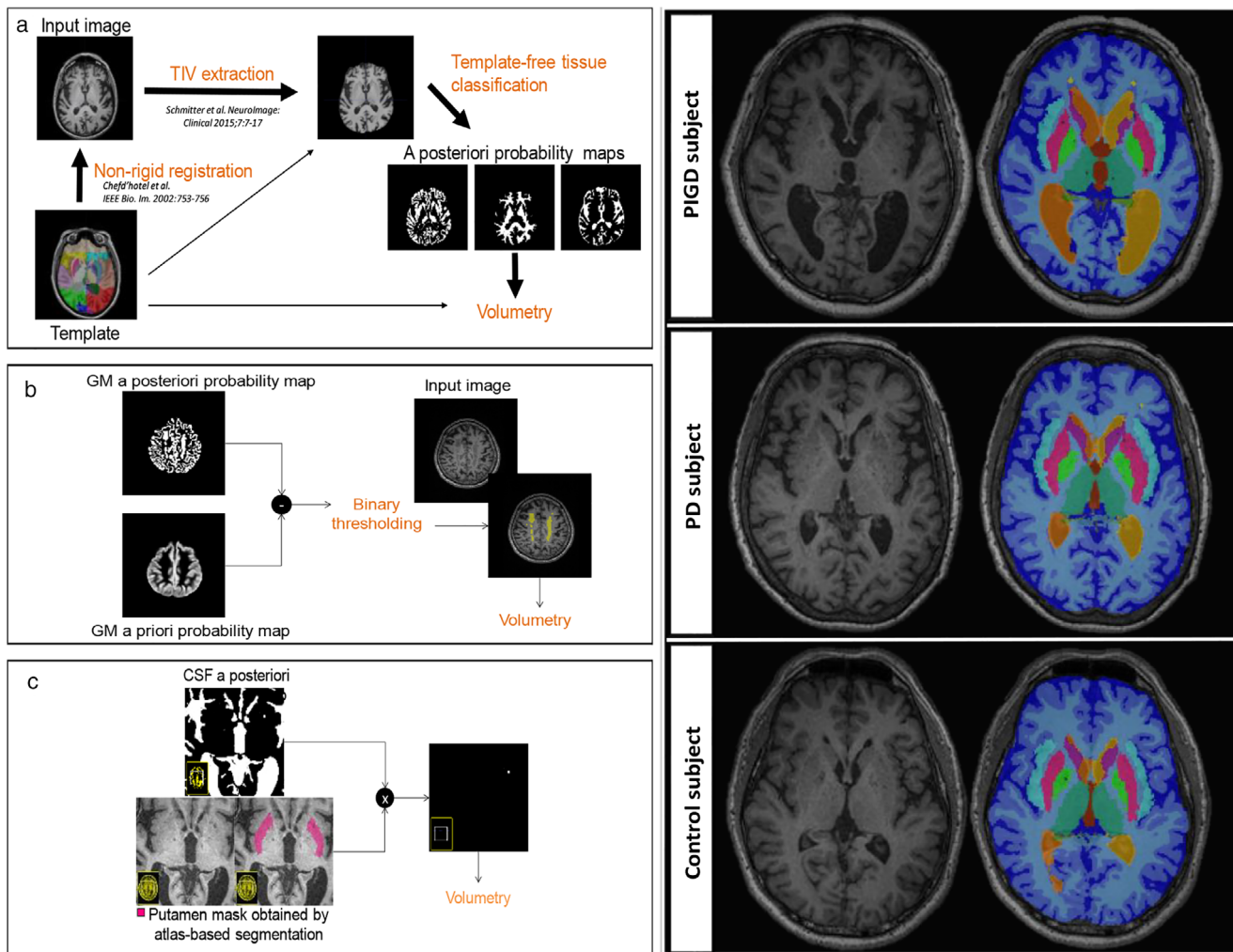
FIGURE 1: MorphoBox processing pipeline (a) generating a posteriori probability maps and volumetry, estimating (b) WMab volume and (c) putamen GMab (eg), (d) illustrative segmentation masks overlaid on axial T$_1$-MPRAGE images of representative PIGD, PD, and HC subjects.

All segmentation masks were reviewed using ITK-Snap.[25] WMab and GMab segmentation was assessed with corresponding FLAIR images of each subject. Quality of the segmentation masks for each subject was independently assessed by two authors (E.F. and C.A.) with about 3 years of experience. When discrepant, consensus was reached with a third reviewer (L.C.) with more than two decades of neuroradiological experience.

Statistical Analysis

Data analysis was performed using R v. 3.4.1 (Vienna, Austria). One-way analysis of variance (ANOVA) on ranks controlling for age and gender with Bonferroni-corrected pairwise comparisons was used to assess significant brain segmentation and clinical parameter differences across subgroups. As aforementioned, estimated volumes were summed over both hemispheres and then normalized by total brain volume to correct for atrophy, prior to intersubject comparisons. Univariate regression was performed to determine the dependence of TBS and UPDRS scores on brain segmentation variables while controlling for age and gender. After variable selection by stepwise regression, a multiple linear regression model, controlled for age and gender, was utilized to assess the relationship between extracted

volumetry and clinical scores. Additionally, logistic regression was performed to differentiate PIGD from PD, and discriminative reliability was evaluated using receiver operating characteristics (ROC) analysis. Statistically significant variables from univariate analysis were converted to indicator variables to form the initial variable set, with forward selection performed to construct the full model in ROC analysis. Unless otherwise stated, statistical significance was defined at $P < 0.05$.

Results

Table 1 summarizes the demographics and clinical characteristics of subjects included in the final analysis. Two PIGD patients were excluded due to significant misclassification of GMab in the striatum. Figure 1d illustrates representative images demonstrating the segmentation output and labeling of both WMab and GMab.

Table 2 details the volumetric comparison of the structures of interest and statistical comparisons between the PIGD, PD, and HC after Bonferroni correction. Lobar analyses (namely, frontal, parietal, temporal, and occipital) of

TABLE 1. Summarized Demographics and Clinical Characteristics

Total included N = 64	PIGD N = 23	PD N = 21	HC N = 20	P-value
Age (years)	72.87 ± 5.69	71.95± 4.80	71.45 ± 4.89	0.42
Range (years)	63~82	62~82	62~80	
Gender (n)				
Male	17	17	16	0.89[+]
Female	6	4	4	
AMT	9.13 ±0.16	9.38 ± 0.17	9.55 ± 0.17	0.21
H&Y	2.76 ± 0.12	2.24 ± 0.12		<0.01
TBS				
Total	16.22 ± 0.83	19.86 ± 0.87	26.65 ± 0.89	<0.01**
Balance	9.35 ± 0.53	11.24 ± 0.56	15.25 ± 0.57	<0.01*
Gait	6.91 ± 0.40	8.62 ± 0.42	11.40 ± 0.43	<0.01**
UPDRS				
Total	43.30 ± 2.96	40.62 ± 3.10		0.53
Tremor	0.43 ± 0.79	4.62 ± 0.83		<0.01
Nontremor	23.04 ± 1.35	18.29 ± 1.41		0.02
Vascular risk Factor (n)				
Diabetes	9	5	3	0.19
Hypertension	11	12	12	0.70
Heart disease	6	3	1	0.18[+]
Hypercholesterolemia	9	9	6	0.68

Values shown as mean ± SE, except for age (SD). P-values derived from one-way ANOVA between-subjects, except for gender and vascular risk factor, which were tested using chi-square test of independence.
AMT = Abbreviated Mental Test; H&Y = Hoehn and Yahr Stage Scale; TBS = Tinetti Balance Scale; UPDRS = Unified Parkinson Disease Rating Scale. PIGD = postural instability gait disorder; PD = Parkinson's disease; HC = healthy controls
[+]P-value was based on 1000 bootstrapped to correct for cell frequency < 5.
*Pairwise comparison after Bonferroni correction were statistically significant (P < 0.05), except for PIGD and PD (P = 0.05).
**All pairwise comparison after Bonferroni correction were statistically significant (P < 0.05)

cortical gray matter and white matter volumetry demonstrated no significant differences between PIGD, PD, and healthy controls (HC), and are not included. Structural volumetry that were significantly different across the groups are graphically depicted in Fig. 2a,b.

Univariate regressions (Table 3) against volumetric data, controlling for age and gender, demonstrated strong statistical significance of WMab, caudate, putamen, and thalamic GMab, and lateral and third ventricular volumes in predicting TBS scores (P < 0.005) in both PIGD and PD. However, regression with a stepwise variable selection method performed on the whole cohort on an initial set of significant variables from univariate regressions showed that caudate GM was the single variable that significantly predicted TBS scores (b = 3.93, t(58) = 2.450, P = 0.017) and also explained 22% of the variance in TBS

scores, R^2 = 0.22, $F(5,58)$ = 3.26, P = 0.01, when adjusted for age and gender. ROC analysis (Fig. 2c) of a model incorporating WMab, caudate GMab, and caudate GM discriminated PIGD with sensitivity = 0.83 and specificity = 0.76 (AUC = 0.84). This structural composite model may aid clinical differentiation of PIGD from PD. Table 4 shows the binary classification results for PIGD and the non-PIGD group.

Discussion

Volumetric findings of the caudate correlate well with severity of gait imbalance in PIGD, but less so with PD. The decrease in caudate gray matter represents a loss of dopaminergic terminals in a key relay nucleus downstream from the substantia nigra in the nigrostriatal pathway.[26] Compared with controls,

TABLE 2. Volumetric Comparison of Selected Structures With P-Values for Post-Hoc Bonferroni-Corrected Comparisons Between the PIGD, PD, and HC

Structure	PIGD	PD	Controls	F-value (P-value)	PIGD vs. PD	PIGD vs. HC	PD vs. HC
Total-intracranial volume	1.000	1.000	1.000	—	—	—	—
CSF	0.315 ± 0.005	0.295 ± 0.005	0.282 ± 0.005	11.945 (0.000)	0.014	<0.001	n.s
Lateral Ventricles	0.053 ± 0.003	0.039 ± 0.003	0.032 ± 0.003	10.867 (0.000)	0.006	<0.001	n.s
3rd Ventricle	0.003 ± 0.000	0.003 ± 0.000	0.003 ± 0.000	7.104 (0.002)	0.029	0.002	n.s
4th Ventricle	0.003 ± 0.000	0.002 ± 0.000	0.002 ± 0.000	5.828 (0.005)	n.s	0.005	n.s
Whole brain	1.000	1.000	1.000	—	—	—	—
GM	0.582 ± 0.005	0.580 ± 0.005	0.584 ± 0.005	0.131 (0.877)	n.s	n.s	n.s
WM	0.418 ± 0.005	0.420 ± 0.005	0.416 ± 0.005	0.131 (0.877)	n.s	n.s	n.s
WMab	0.010 ± 0.002	0.003 ± 0.002	0.002 ± 0.002	7.509 (0.001)	0.006	0.003	n.s
Thalamus volumetry	0.013 ± 0.000	0.014 ± 0.000	0.013 ± 0.000	1.661 (0.199)	n.s	n.s	n.s
Thalamus GM	0.378 ± 0.026	0.475 ± 0.028	0.433 ± 0.028	3.251 (0.046)	0.041	n.s	n.s
Thalamus WM	0.610 ± 0.026	0.516 ± 0.027	0.559 ± 0.028	3.107 (0.052)	0.047	n.s	n.s
Thalamus GMab	0.012 ± 0.001	0.009 ± 0.001	0.009 ± 0.001	4.337 (0.017)	0.036	n.s	n.s
Caudate volumetry	0.010 ± 0.000	0.009 ± 0.000	0.008 ± 0.000	12.714 (0.000)	n.s	<0.001	0.029
Caudate GM	0.843 ± 0.012	0.893 ± 0.013	0.876 ± 0.013	4.228 (0.019)	0.018	n.s	n.s
Caudate WM	0.141 ± 0.012	0.095 ± 0.012	0.113 ± 0.013	3.682 (0.031)	0.028	n.s	n.s
Caudate GMab	0.016 ± 0.001	0.011 ± 0.001	0.011 ± 0.001	5.442 (0.007)	0.019	0.019	n.s
Putamen volumetry	0.013 ± 0.000	0.013 ± 0.000	0.013 ± 0.000	1.637 (0.203)	n.s	n.s	n.s
Putamen GM	0.568 ± 0.028	0.631 ± 0.029	0.569 ± 0.030	1.584 (0.214)	n.s	n.s	n.s
Putamen WM	0.417 ± 0.027	0.362 ± 0.029	0.425 ± 0.029	1.415 (0.251)	n.s	n.s	n.s
Putamen GMab	0.015 ± 0.003	0.007 ± 0.003	0.006 ± 0.003	2.919 (0.062)	n.s	n.s	n.s
Global pallidus volumetry	0.004 ± 0.000	0.004 ± 0.000	0.004 ± 0.000	2.763 (0.071)	n.s	n.s	n.s
Globus pallidus GM	0.098 ± 0.015	0.087 ± 0.016	0.087 ± 0.016	0.154 (0.858)	n.s	n.s	n.s
Globus pallidus WM	0.889 ± 0.017	0.903 ± 0.018	0.907 ± 0.019	0.287 (0.752)	n.s	n.s	n.s
Globus pallidus GMab	0.014 ± 0.005	0.010 ± 0.005	0.006 ± 0.005	0.658 (0.522)	n.s	n.s	n.s

CSF = cerebrospinal fluid; GM = gray matter; WM = white matter; WMab = white matter lesion load; GMab = deep gray nuclear lesion load; n.s = not significant.
Except for CSF, which is expressed as a fraction of total-intracranial volume; all other values are expressed as fractions of volumes as detailed in the Methods section.
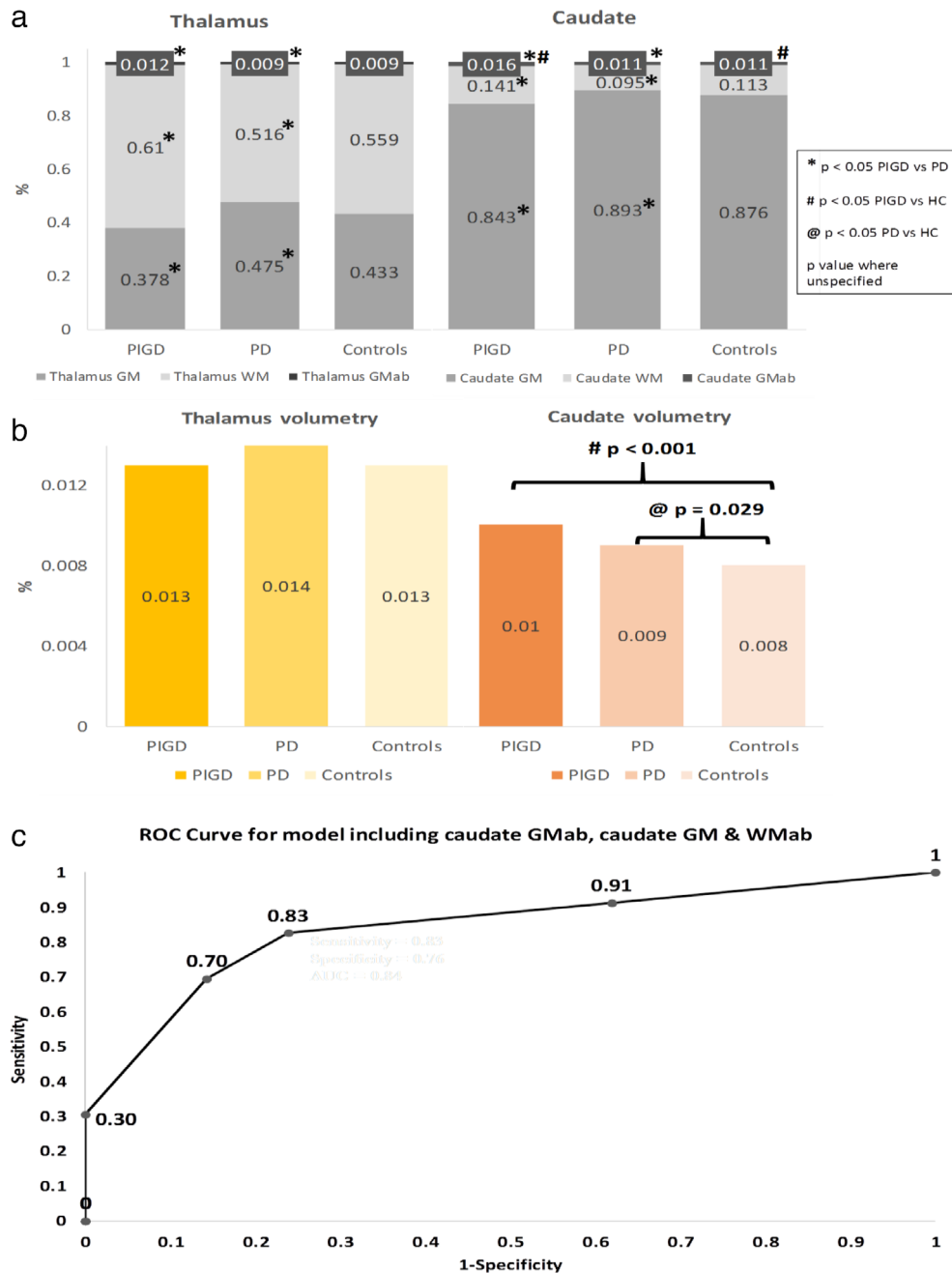
FIGURE 2: Graphical depiction of thalamic and caudate (a) tissue compositions, (b) volumetry with comparisons between groups, and (c) area under the ROC curve for composite model predicting PIGD classification as 0.84.

caudate volumes were increased in our PD and PIGD patients, reflecting greater global brain atrophy relative to the caudate, as also reported by others.[27] Striatal atrophy has been reported to occur early in the disease and plateauing thereafter.[10,28,29] However, we found no significant atrophy of the putamen in our patients, which may be due to variations in morphometric methodology and patient populations.

Apart from neuronal loss in the striatum, white matter abnormalities are known to affect postural stability and gait motor functions in PD[30,31] by disrupting important subcortical afferents,[30] corticostriatal–thalamocortical loops,[32] and interhemispheric connections of the corpus callosum,[15,33] which are critical for complex integrated motor programs. This is particularly true for periventricular white matter abnormalities, which are known to be more prevalent in PIGD than in PD and HC.[28,30] Further research is needed to investigate how periventricular white matter lesions and caudate abnormalities increase disruption to the neuromodulator projection systems, with greater adverse impact on gait and balance motor scores.

To date, most PD-related morphometric studies have focused on regional gray matter volume changes using a voxel-based morphometry approach.[10,12,14,34] However, classification performance from a multivariate volume-based morphometric approach has shown comparable or superior results over whole-

TABLE 3. Selected Univariate Analysis of Dependence of TBS on Segmented Brain Structures, Controlling for Age and Gender in PIGD and PD

Structure	Unstandardized beta	Standardized beta	P value for unstandardized beta	R^2
CSF	−0.575	−0.293	0.034*	0.156
Lateral ventricles	−123.511	−0.410	0.003*	0.220
3rd Ventricle	−2737.742	−0.424	0.002*	0.220
4th Ventricle	−2447.636	−0.316	0.013*	0.180
GM	12.544	0.055	0.687	0.093
WM	−12.544	−0.055	0.687	0.093
WMab	−274.422	−0.399	0.001*	0.235
Thalamus volumetry	347.466	0.057	0.659	0.093
Thalamus GM	11.110	0.264	0.044*	0.150
Thalamus WM	−10.883	−0.256	0.051	0.147
Thalamus GMab	−530.621	−0.342	0.005*	0.204
Caudate volumetry	−2432.866	−0.550	<0.001*	0.319
Caudate GM	29.248	0.322	0.014*	0.178
Caudate WM	−28.068	−0.298	0.023*	0.166
Caudate GMab	−398.252	−0.366	0.003*	0.216
Putamen volumetry	−767.086	−0.166	0.235	0.111
Putamen GM	0.368	0.009	0.947	0.090
Putamen WM	1.405	0.034	0.801	0.091
Putamen GMab	−143.504	−0.360	0.003*	0.216
Globus pallidus volumetry	257.412	0.015	0.913	0.090
Globus pallidus GM	−6.393	−0.079	0.535	0.096
Globus pallidus WM	6.771	0.096	0.448	0.099
Globus pallidus GMab	−28.150	−0.108	0.403	0.101

CSF = cerebrospinal fluid; GM = gray matter; WM = white matter; WMab = white matter lesion load; GMab = deep gray nuclear lesion load.
*Significant P values <0.05

brain voxel-based morphometry approaches[24] in neurodegenerative disorders. In addition, our approach incorporated lesional WMab in the whole-brain analysis, accounting for periventricular white matter abnormalities, which are important pathological substrates in PIGD.[28,31,35]

Segmentation of GMab revealed differential involvement in our study groups. GMab is conceived as a T_1 hypointense component within the deep gray matter nuclei anatomical masks and represents neuronal changes or degeneration with loss of dopaminergic terminals. On balance of evidence, the statistical significance in GMab difference across all three subgroups, the high sensitivity of GMab in the ROC

analysis and the improved discriminative power in the ROC analysis when GMab is included suggests that GMab is a significant contributor to the nigrostriatal pathway disruption[7] besides conventional caudate GM volumetry and WMab in PIGD. Further work needs to be done to validate and apply this GMab estimation approach to other neurological disorders that affect deep gray matter nuclei.

We acknowledge several limitations in this study. First, we are cognizant that precise fidelity in automated classification of periventricular white matter and deep gray nuclear lesions remains challenging.[36,37] For example, Fig. 1d illustrates minor misclassification of periventricular white matter

TABLE 4. Binary Multivariate Classification Results for PIGD and Non-PIGD (including HC) Subjects in Relation to TBS Scores

Classification rule	AUC	SEN	SPE	BACC	PPV	NPV	LP+	LR–	DeLong's test	McNemar test
WMab only	0.753	0.696	0.810	0.753	0.800	0.708	3.652	0.376	0.038	0.221
Caudate GM only	0.670	0.435	0.905	0.670	0.833	0.594	4.565	0.625	0.017	0.001
Caudate GMab only	0.671	0.913	0.429	0.671	0.636	0.818	1.598	0.203	0.001	0.008
Combined	0.840	0.826	0.762	0.794	0.792	0.800	3.470	0.228		

The following performance measures are reported: SEN = sensitivity; SPE = specificity; BACC = balanced accuracy (average of sensitivity and specificity); PPV = positive predictive value; NPV = negative predictive value; LR+ = positive likelihood ratio; LR– = negative likelihood ratio. *P*-values are reported for DeLong's and McNemar tests (with combined model as reference).

lesions and residual gliotic hypointensities partly due to their close proximity to the ventricles.[36]

Second, tissue classification of the deep gray nuclei into gray and white matter components can be further refined. At present, the atlas-free tissue classification algorithms in MorphoBox use the signal intensity of the deep gray nucleus to determine the white matter component and then parcellate it into each basal ganglia structure using atlas-based segmentation. The small volume of these deep gray nuclei makes them vulnerable to partial volume averaging from surrounding white matter. Furthermore, neuronal loss with aging may also contribute to the computed white matter component at the subcellular level. Nevertheless, we demonstrated good results with the fast segmentation that allowed group discrimination of PIGD, further supporting the concept that high standards of exactitude are probably not a prerequisite in morphometric disease classification[24] to aid the clinician in diagnosis. Notwithstanding, further multimodal segmentation approaches incorporating relevant sequences (eg, T_2W or FLAIR) may offer promise to account for all brain lesions with improved accuracy.[37] Third, cognitive and neuropsychiatric symptoms were not evaluated in our study. Nevertheless, there were no significant differences in lobar volumetric analyses of WM and cortical GM volumetry in our results.

In conclusion, using a multivariate volume-based morphometry algorithm to derive white matter and deep gray nuclear lesion load, differential neuronal loss in key relay nuclei and white matter circuitry identified and correlated with gait imbalance severity. This allowed differentiation of the PIGD motor subtype from PD. The speed and unbiased discriminative power of this fully automated segmentation algorithm offers potential as a complement to clinical assessments and may support diagnosis and stratification of PD patients into relevant subtypes for better disease management.

Acknowledgment

References

1. Jankovic J, McDermott M, Carter J, et al. Variable expression of Parkinson's disease: A base-line analysis of the DATATOP cohort. The Parkinson Study Group. Neurology 1990;40:1529–1534.

2. Fereshtehnejad SM, Postuma RB. Subtypes of Parkinson's disease: What do they tell us about disease progression? Curr Neurol Neurosci Rep 2017;17:34.

3. Hutchinson M, Raff U. Structural changes of the substantia nigra in Parkinson's disease as revealed by MR imaging. AJNR Am J Neuroradiol 2000;21:697–701.

4. Nagae LM, Honce JM, Tanabe J, Shelton E, Sillau SH, Berman BD. Microstructural changes within the basal ganglia differ between Parkinson disease subtypes. Front Neuroanat 2016;10:17.

5. Graham JM, Paley MNJ, Grünewald RA, Hoggard N, Griffiths PD. Brain iron deposition in Parkinson's disease imaged using the PRIME magnetic resonance sequence. Brain 2000;123:2423–2431.

6. Wang JY, Zhuang QQ, Zhu LB, et al. Meta-analysis of brain iron levels of Parkinson's disease patients determined by postmortem and MRI measurements. Sci Rep 2016;6:36669.

7. Schneider E, Ng KM, Yeoh CS, et al. Susceptibility weighted MRI of extrapyramidal brain structures in Parkinsonian disorders. Medicine 2016;95:e3730.

8. Rajput AH, Pahwa R, Pahwa P, Rajput A. Prognostic significance of the onset mode in parkinsonism. Neurology 1993;43:829–830.

9. Burn DJ, Rowan EN, Allan LM, Molloy S, O'Brien JT, McKeith IG. Motor subtype and cognitive decline in Parkinson's disease, Parkinson's disease with dementia, and dementia with Lewy bodies. J Neurol Neurosurg Psychiatry 2006;77:585–589.

10. Lewis MM, Du G, Lee EY, et al. The pattern of gray matter atrophy in Parkinson's disease differs in cortical and subcortical regions. J Neurol 2016;263:68–75.

11. Burton EJ, McKeith IG, Burn DJ, Williams ED, O'Brien JT. Cerebral atrophy in Parkinson's disease with and without dementia: A comparison with Alzheimer's disease, dementia with Lewy bodies and controls. Brain 2004;127:791–800.

12. Jia X, Liang P, Li Y, Shi L, Wang D, Li K. Longitudinal study of gray matter changes in Parkinson cisease. AJNR Am J Neuroradiol 2015;36: 2219–2226.

13. Weintraub D, Doshi J, Koka D, et al. Neurodegeneration across stages of cognitive decline in Parkinson disease. Arch Neurol 2011; 68:1562–1568.

14. Rosenberg-Katz K, Herman T, Jacob Y, Kliper E, Giladi N, Hausdorff JM. Subcortical volumes differ in Parkinson's disease motor subtypes: New insights into the pathophysiology of disparate symptoms. Front Hum Neurosci 2016;10:356.

15. Chan LL, Ng KM, Rumpel H, Fook-Chong S, Li HH, Tan EK. Trans-callosal diffusion tensor abnormalities in predominant gait disorder parkinsonism. Parkinsonism Relat Disord 2014;20:53–59.

16. Tan WQ, Yeoh CS, Rumpel H, et al. Deterministic tractography of the nigrostriatal-nigropallidal pathway in Parkinson's disease. Sci Rep 2015;5:17283.

17. Tolosa E1, Wenning G, Poewe W. The diagnosis of Parkinson's disease. Lancet Neurol 2006;5:75–86.

18. Stebbins GT, Goetz CG, Burn DJ, Jankovic J, Khoo TK, Tilley BC. How to identify tremor dominant and postural instability/gait difficulty groups with the movement disorder society unified Parkinson's disease rating scale: Comparison with the unified Parkinson's disease rating scale. Mov Disord 2013;28:668–670.

19. Fahn S, Elton R. The Unified Parkinson's Disease Rating Scale. In: Fahn S, Marsden C, Calne D, Goldstein M, eds. *Recent developments in Parkinson's Disease*. 2. Florham Park, NJ: Macmillan Health Care Information; 1987. p 153–163.

20. Goetz CG, Poewe W, Rascol O, et al. Movement disorder society task force report on the Hoehn and Yahr staging scale: Status and recommendations. Move Disord 2004;19:1020–1028.

21. Tinetti ME. Performance-oriented assessment of mobility problems in elderly patients. J Am Geriatr Soc 1986;34:119–126.

22. Hodkinson HM. Evaluation of a mental test score for assessment of mental impairment in the elderly. Age Ageing 1972;1:233–238.

23. Maréchal B, Roche A, Kober T, et al. (eds.). Automated evaluation of deep gray matter neuronal damage in multiple sclerosis patients. In: Proc 25th Annual Meeting ISMRM, Honolulu; 2017.

24. Schmitter D, Roche A, Marechal B, et al. An evaluation of volume-based morphometry for prediction of mild cognitive impairment and Alzheimer's disease. Neuroimage Clin 2015;7:7–17.

25. Yushkevich PA, Piven J, Hazlett HC, et al. User-guided 3D active contour segmentation of anatomical structures: Significantly improved efficiency and reliability. Neuroimage 2006;31:1116–1128.

26. Lee SH, Kim SS, Tae WS, et al. Regional volume analysis of the Parkinson disease brain in early disease stage: Gray matter, white matter, striatum, and thalamus. AJNR Am J Neuroradiol 2011;32:682–687.

27. Almeida OP, Burton EJ, McKeith I, Gholkar A, Burn D, O'Brien JT. MRI study of caudate nucleus volume in Parkinson's disease with and without dementia with Lewy bodies and Alzheimer's disease. Dement Geriatr Cogn Disord 2003;16:57–63.

28. Herman T, Rosenberg-Katz K, Jacob Y, et al. White matter hyperintensities in Parkinson's disease: Do they explain the disparity between the postural instability gait difficulty and tremor dominant subtypes? PLoS One 2013;8:e55193.

29. Maetzler W, Liepelt I, Berg D. Progression of Parkinson's disease in the clinical phase: Potential markers. Lancet Neurol 2009;8:1158–1171.

30. Bohnen NI, Albin RL. White matter lesions in Parkinson disease. Nat Rev Neurol 2011;7:229–236.

31. Lee SJ, Kim JS, Lee KS, et al. The severity of leukoaraiosis correlates with the clinical phenotype of Parkinson's disease. Arch Gerontol Geriatr 2009;49:255–259.

32. Alexander GE, DeLong MR, Strick PL. Parallel organization of functionally segregated circuits linking basal ganglia and cortex. Annu Rev Neurosci 1986;9:357–381.

33. Gattellaro G, Minati L, Grisoli M, et al. White matter involvement in idiopathic Parkinson disease: A diffusion tensor imaging study. AJNR Am J Neuroradiol 2009;30:1222–1226.

34. Nyberg EM, Tanabe J, Honce JM, et al. Morphologic changes in the mesolimbic pathway in Parkinson's disease motor subtypes. Parkinsonism Relat Disord 2015;21:536–540.

35. Levy-Cooperman N, Ramirez J, Lobaugh NJ, Black SE. Misclassified tissue volumes in Alzheimer disease patients with white matter hyperintensities: Importance of lesion segmentation procedures for volumetric analysis. Stroke 2008;39:1134–1141.

36. Nakamura K, Fisher E. Segmentation of brain magnetic resonance images for measurement of gray matter atrophy in multiple sclerosis patients. Neuroimage 2009;44:769–776.

37. Griffanti L, Zamboni G, Khan A, et al. BIANCA (Brain Intensity AbNormality Classification Algorithm): A new tool for automated segmentation of white matter hyperintensities. Neuroimage 2016;141:191–205.